British Journal of Cancer www.nature.com/bjc

ARTICLE OPEN

Check for updates

Translational Therapeutics Colour

Spatial molecular analyses reveal key features associated with response to KN026 in advanced HER2-positive breast cancer

Jianli Ma[1,5], Shengnan Sun[2,5], Xiaowen Tang[3], Jingxuan Wang[2], Wenhui Zhao[2], Dabei Tang[2], Ying Song[2], Liru Li[2], Haitao Luo[4], Xuhui Liu[4], Yuwei Deng[2✉] and Qingyuan Zhang[2✉]

BACKGROUND: KN026 is a novel bispecific HER2-targeting antibody for HER2-positive recurrent or metastatic breast cancer that showed prolonged median PFS and lessened distinction of PFS regarding the HR subgroup in our phase II clinical trial, compared with PUFFIN study of first-line trastuzumab combined with pertuzumab therapy. A more detailed discovery of its peculiarity is needed for optimal application of KN026 treatment.

METHODS: We performed whole-transcriptome sequencing of digital spatial profiling (DSP) on 8 pre/post-treatment tumor samples. Mechanistic explorations were conducted by plasmid transfection, co-culture, CCK8 proliferation assay and flow cytometry.

RESULTS: Compared to the tumor regions with non-objective response (OR), those with OR had high expression of *CALML5*, *TFAP2B*, and *ERBB2*, and relatively low expression of *ESR1* in tumor cells at baseline. The expression of *ESR1* had a tentative association with PI3K/AKT and NOTCH signaling pathways which were downstream or interactive pathways of HER2 target and also acted as interactive pathways of ER-mediated signaling. The co-expression of *ERBB2* and *CDK12* emerged as a distinctive signature of OR. KN026 treatment also reshaped intratumoral activated T- and B-cell subtypes in hot-tumor regions, regardless of myeloid-derived cells.

CONCLUSIONS: Both HER2 and ESR1 are determinant of KN026 efficacy in advanced HER2-positive breast cancer, implying the potential of KN026 combined with endocrine therapy in HER2- and ER-positive breast cancer.

British Journal of Cancer (2026) 134:685–696; https://doi.org/10.1038/s41416-025-03287-9

BACKGROUND

Breast cancer remains the predominant malignancy among women globally and a principal cause of cancer-related death. GLOBOCAN 2022 data suggest that the incidence and mortality of breast cancer in females were, respectively 23.8% and 15.4%, with 9.7 million new cases [1]. Notably, human epidermal growth factor receptor 2 (HER2)-positive breast cancer accounts for 15%-20% of these cases [2]. Established therapies for HER2-positive recurrent or metastatic cases such as trastuzumab, pertuzumab, tyrosine kinase inhibitors (TKIs; e.g., lapatinib, neratinib), and especially antibody drug conjugates (ADCs; e.g., T-DM1, and DS8201a), have offered abundant prognostic benefits [3]. KN026, a novel bispecific antibody binding to the same extracellular region of target proteins as trastuzumab (TZB, domain IV) and pertuzumab (PZB, domain II), achieves 'dual HER2 blockade'. The promise of KN026 was confirmed in a prior phase I clinical trial (NCT03619681; ORR, 28.1%; mPFS, 6.8 months) [4] and especially our leading phase II clinical trial (CTR20192289; ORR, 76.4%; mPFS, 27.7 months) [5]. Our findings are in agreement with previously reported ORR values of 79% in both PERUSE and PUFFIN studies using respective PZB, TZB, and docetaxel regimens, with significantly prolonged PFS compared with the CLEOPATRA, PERUSE, and PUFFIN studies [6–8]. Its challenge achievement raises critical question regarding the superior effects on HER2 target and needs to be further investigated.

Preclinical and clinical studies support strategies promoting HER2 receptor internalization [9], retaining antibody-dependent cellular cytotoxicity and phagocytic killing effect [10], as well as intensive blockage of ligand-dependent or independent tumor growth [4]. There is evidence that targeted therapy induces acquired alterations, especially in HER2 signaling, which shift the balance within tumor cells and presents with multiple responses [11]. Subgroup analyses in our phase II clinical trial demonstrated better median PFS in cohorts with baseline HER2 IHC3+ finding, while stratified by baseline HR (ER and/or PR) status indicated little survival distinction between two subgroups [5]. The survival

[1]Department of Radiation Oncology, Harbin Medical University Cancer Hospital, Harbin, Heilongjiang Province, PR China. [2]Department of Medical Oncology, Harbin Medical University Cancer Hospital, Harbin, Heilongjiang Province, PR China. [3]Department of Medical, Jiangsu Alphamab Biopharmaceuticals Co. Ltd., Suzhou, Jiang Su, PR China. [4]Department of Medical Sciences, Kindstar Global Precision Medicine Institute, Shenzhen, PR China. [5]These authors contributed equally: Jianli Ma, Shengnan Sun.
✉email: dengyuweidoctor@outlook.com; 0566@hrbmu.edu.cn

Received: 14 May 2025 Revised: 22 October 2025 Accepted: 14 November 2025
Published online: 9 December 2025

benefit of KN026 had no distinct bias regarding HR status but showed better results than that in PUFFIN study [12]. This manifestation underscored the necessity of deciphering the intertwined effects of molecular interactions between patients with distinct responses to KN026 treatment, thus presenting an intriguing topic [13].

We conducted quantitative and high-plex mRNA analysis in spatially defined tumor regions from HER2-positive recurrent/metastatic breast cancer samples before and after 2 cycles of KN026 treatment using digital spatial profiling (DSP, NanoString Biotechnology). We uncover the underpinning of responsive or non-responsive to KN026 therapy that indicates an ERBB2-centered network in tumor cells, identify responsive immune cell subtypes to KN026, and suggest the potential combination of endocrine therapy and KN026 in HER2- and HR-positive recurrent/metastatic breast cancer.

MATERIALS AND METHODS

Patients and study population

Samples were obtained from patients with recurrent/metastatic HER-2 positive breast cancer who were enrolled in our phase II multicenter clinical trial, during which they were treated with KN026 combined with docetaxel in 21-day cycles (ClinicalTrials.gov, registration number: NCT05838066, safety set) and had provided written informed consent. This study was approved by the Institutional Review Board of Harbin Medical University Cancer Hospital (Ethics No. 2019-180) [5]. The Response Evaluation Criteria in Solid Tumors Version 1.1 framework was adopted to evaluate the response to treatments [14]. The formalin-fixed, paraffin-embedded tumor tissue samples from biopsies were collected at baseline (within 1 week before treatment initiation) and after two cycles of treatment (after 6 weeks of treatment). Samples were stained with hematoxylin and eosin (H&E) for confirmation of morphology, and then processed and analyzed using a GeoMx Digital Spatial Profiler.

Sample preparation and in situ hybridization

The study design comprised eight specimens from six patients (3 with objective response (OR), 3 with non-OR) included all pre-treatment samples ($n = 6$) and 2 paired post-treatment samples (1 from OR within tumor sites, 1 from non-OR). The slides were deparaffinized and rehydrated followed by washes with CitriSolv, in 100% ethanol, 95% ethanol, and phosphate-buffered saline (PBS). Then, antigen retrieval was performed using aqueous diethylpyrocarbonate at 99 °C for 10 s followed by treatment with 1× Tris-EDTA at 99 °C for 20 min. Then, the slides were incubated with proteinase K solution on a BOND RXm autostainer (Leica) to expose RNAs. The slides were post-fixed with 10% neutral buffered formalin (NBF). Then, in situ hybridization was performed as described with 4 nM UV-photocleavable oligo probes of 1812 mRNA transcripts (median 10 probes per target) (Cancer Transcriptome Atlas, CTA) [15]. After washing, the slides were stained for the morphological markers pan-cytokeratin (PanCK, AE1 + AE3, Novus Biologicals), CD20 (MEM-97, Novus Biologicals), and CD3 (UMAB54, OriGene labeled with Alexi Fluor 647), while nuclei were counter stained with SYTO 13 (NanoString, 121300310) at 4°C overnight in a humidity chamber. The signals were examined using the GeoMx instrument.

GeoMx™ digital spatial profiling

Continuous sections, pre-screened via hematoxylin and eosin (HE) staining, were selected for Nanostring digital spatial profiling (DSP) analysis. The technical procedure has been detailed previously (Merritt et al., https://doi.org/10.1038/s41587-020-0472-9). The GeoMx Whole Transcriptome Atlas (WTA) panel, encompassing 18,677 genes, was employed for targeted mRNA expression profiling. Oligonucleotide-tagged probes from the WTA panel were incubated with the tissue sections to perform in situ hybridization. Subsequently, tissue sections were stained using the GeoMx Solid Tumor TME Morphology Kit (Nanostring) to distinguish distinct compartments: panCK for epithelial cells, CD3 for T cells, CD20 for B cells, and Syto13 for DNA. Pathologists discriminated between normal and cancerous epithelial cells based on histological morphology. Regions of interest (ROIs) were selected and assessed by pathologists. Oligonucleotide tags derived from the minimal illumination area or area of interest (AOI) were excised and harvested via ultraviolet light irradiation. A total of two types of AOIs were collected: the epithelial cell compartment (PanCK +) and the stromal compartment (PanCK-). In accordance with the manufacturer's instructions (NanoString), the oligonucleotide tags were processed for library construction, sequencing, and digital quantification using the DNBSEQ-T7 platform.

Data processing and analysis

Analysis was performed on the GeoMx DSP Control Center using the Data Analysis module V.2.4.0.421. For quality control (QC), the regions of interest (ROIs) were removed from the analysis when the reads and templates were less than 80% identical. Nuclei counts (>100) and surface area (>8000 square micrometers) defined ROIs where area normalization and different cell numbers were used for size adjustment.

The numbers of immune and stromal cells in the tumor microenvironment were calculated based on 14 immune cell signatures by deconvolution using SpatialDecon V.1.2.0. The equation of $\sqrt[n]{(X1+1)\ldots(X2+1)\ldots(Xn+1)}$ was used for evaluating signature scores. Genes with low expression levels were filtered using the 'filterByExpr' function at parameter 'min.count=3' using the edgeR package (V.3.34.0). Differentially expressed genes (DEGs) were identified using the glmFit, glmLRT, estimateGLMCommonDisp, estimateGLMTrendedDisp, and estimateGLMTagwiseDisp functions based on the criteria | log2FoldChange | >1 and false discovery rate <0.05. The enrichment of DEGs was calculated using KOBAS-i. The corresponding RNAs in all AOIs (tumor, stromal, or immune cells) were calculated using the equation: average value = (X1 + X2 + ……Xn)/N, where N is the number of AOIs in each sample.

Cell culture and reagents

The human cell line MCF7-HER2 (ATCC code: AC102316) was obtained from the American Type Culture Collection (Manassas, VA, USA) and was cultured in Dulbecco's modified Eagle medium (DMEM) supplemented with 10% heat-inactivated fetal bovine serum (FBS) and 1% penicillin-streptomycin-glutamine (PSG) at 37 °C in a humidified incubator with 5% CO_2. BT474 cells were from the same source and were cultured in Roswell Park Memorial Institute (RPMI)-1640 medium containing 10% FBS. KN026 was obtained from Alphamab Biopharmaceuticals Co., Ltd. (Suzhou, China), tamoxifen was obtained from MedChemExpress (Shanghai, China), and trastuzumab/pertuzumab was obtained from Roche (Shanghai, China).

Cell transfection

The plasmid encoding human CDK12 (pLV3-CMV-CDK12(human)-3×FLAG-CopGFP-Puro) was synthesized by Aopeng Biotechnology Co., Ltd. (Shanghai, China). For overexpressing CDK12, BT474 cells were seeded into 6-well plates, followed by transfection with pLV3-CMV-CDK12(human)-3×FLAG-CopGFP-Puro and pLV3-CMV-NC (human)-3×FLAG-CopGFP-Puro plasmids using polyethyleneimine (Polysciences, Inc., Warrington, PA, USA) when the cells reached 70–80% confluence. Following 72 h after transfection, the cells were collected for western blotting as previously described (14) using a rabbit antibody against CDK12 (1:1000; ABclonal, Wuhan, China). The transfected cells were then incubated with puromycin (1 mg/L) for five days to select stable clones.

Western blot analysis

Cells were lysed with M-PER mammalian protein extraction reagent (Thermo Scientific, Waltham, MA, USA) supplemented with a protease inhibitor cocktail (P1005; Beyotime Biotechnology). Proteins were resolved by SDS–polyacrylamide gel electrophoresis and then transferred to polyvinylidene difluoride membranes. The membranes were blocked with blocking buffer and incubated with the respective antibodies in 3% bovine serum albumin/Tris-buffered saline with Tween-20 at 4 °C overnight, followed by incubation with the secondary antibody at room temperature for 1 h. The protein signals were detected by the electro-chemi-luminescence method.

Co-culture assay

Purification of CD3 + T cells from peripheral blood of healthy donors was achieved with EasySep Human T Cell Isolation Kit (STEMCELL, Vancouver, Canada, Cat#17951) following the manufacturer' s instruction. Subsequently, the acquired T cells were co-cultured with BT474 tumor cells at a ratio of 10:1 for 48 h with or without KN026 treatment (100 mg/L) to assess immune alterations and tumor cell proliferation, maintained in RPMI-1604 containing 10% FBS and 1% penicillin/streptomycin.

Flow cytometry

Flow cytometry of T cell phenotypes was conducted on FACS Cantoll and FACS Aria Fusion instrument (BD) and analysis was performed by FlowJo analysis software (Tree Star). Staining was performed at 4 °C in the presence of Fc block (2.4G2) in cell-staining buffer (PBS + 0.5% BSA + 2 mM EDTA). The primary antibodies were used as following: anti-human APC CD279/PD-1 [EH12.2H7, elabscience], PerCP/Cyanine5.5 CD8a [OKT-8, elabscience], FITC CD4 [SK3, biolegend], APC/Cy7 TCR Vα7.2 [3C10, biolegend]. Then, cells were fixed and permeabilized (No. 554714, BD) for intracellular protein staining using anti-human PE perforin [dG9, biolegend], PE/Cyanine7 Granzyme B recombinant antibody [QA16A02, biolegend]. Brefeldin A (BFA, eBioscience™, 00-4506-51) was added before detection for inhibition of cytokine secretion.

CCK-8 assay

The Cell Counting Kit-8 (CCK8) assay (Beyotime Institute of Biotechnology, Jiangsu, China) was performed to determine the proliferation capacity of tumor cells after treatment with KN026 (100 mg/L), tamoxifen (1 μM), trastuzumab (20 μg/ml), and pertuzumab (20 μg/ml). Cells (4×10^3 per well) were seeded into 96-well plates in six replicates per group. After 7 or 21 days of cultivation, 10 μL of CCK8 solution was added to each well followed by incubation for 2 h. After discarding the supernatant, washing, and dissolving the formazan crystals, the absorbance at 450 nm was measured using a SpectraMax M5 microplate reader.

Statistical analysis

Except for the algorithms described above, statistical analyses were performed in using R statistical software (v4.2.0) and GraphPad Prism Version 9.0 software (GraphPad Software Inc, San Diego, CA). All statistical tests with p-values < 0.05 were considered statistically significant. Mann-Whitney non-parametric two-tailed unpaired t-test was used for between-group gene expression comparisons, while two-way ANOVA with Geisser-Greenhouse correction and Tukey's multiple comparison tests were used for the cell proliferation assay.

RESULTS

Spatial gene expression profiling of KN026-treated tumor regions

In this study, we utilized digital spatial gene expression profiling of 3 tumor tissues from patients with OR and 3 from non-OR at baseline. Simultaneously, the matched samples after 2 cycles of treatment with available tumor sites from one of the patients with OR and one of the patients with a non-response tumor were also analyzed (Table S1).

Serial sections were stained simultaneously with fluorescently labeled antibodies specific for the leukocyte markers CD3 and CD20, epithelial cell marker PanCK, combined with the nuclear stain SYTO 13 for DSP. At the tumor core, regions of interest (ROI, $n = 29$) were selected and refined areas of interest (AOI, $n = 59$) were further cleaved and sequenced. Utilizing the ImmCellAI algorithm (doi: 10.1002/advs.201902880.), a single, publicly available single-cell RNA sequencing dataset (GSE228499) was used as a reference dataset. Through the method of deconvolution and adopting a high-confidence threshold, the composition of malignant tumor cells and other cell subsets in each AOI was determined.

Divide each ROI of hot tumors, cold tumors, and tertiary lymphoid structures (TLS) into areas of interest (AOIs) of malignant (PanCK +) and non-malignant region (CD3+, CD20+, etc.) through ultraviolet segmentation (Fig. 1a, b). Analyze the features of all AOIs using a variety of dimensionality reduction algorithms. Differences were also observed between samples with OR and non-OR at baseline, as well as between pre- and post-treatment samples, reflecting distinctive transcription profiles within spatio-temporal compartments (Fig. S1A-C). We also observed a significant decrease in components of total immune activation markers (*IGHG1*, *B2M*, *HLA-B*) after treatment (Fig. S1D). Distinct epithelial malignant cell, stromal cell, and lymphocyte types were annotated using the marker genes *CEACAM1* and *CALML5* for malignant epithelial cells, *PDGFC* for CAF and *IGHG3* for B lymphocytes (Fig. 1b, Tables S2, S3 and S4). Lymphocytes presented clustered locations within 'hot' tumor regions (highly immune-infiltrated) and tumor sites with OR, while epithelial and stromal cells were clustered in cold tumor regions with non-OR (Fig. 1c and Table S5). Correspondingly, the malignant marker gene expression (e.g. *ESR1*, *ECM1*) was upregulated in tumors with non-OR rather than those with OR (log2 (Fold Change) > 1; Fig. 1d). To determine the pattern of multicellular associations, a spatial covariation matrix was generated across all ROIs of all cell types. A high degree of correlation was generally observed between class-switched memory B cells and M1 macrophages, γδ T-cells and pDC, especially in stromal cell clusters including fibroblasts, as well as cDCs or M2-like macrophages and T-cell subtypes (e.g. T helper 1 and $CD8^+$ central memory T cells). Interestingly, there were week correlations between malignant epithelial cells and other cell types, only obvious with B cells, pDCs, neutrophils and Tregs (Fig. 1e). These results highlight the distinct nature of therapeutically responsive tumor compartments with unique transcriptomic profiles that are plastic across patients.

Tumor cells adapt distinct states in response to KN026 treatment

We proceeded to re-stratified patients with HR status among HER+ subpopulations in our phase II clinical trial [5] and showed relatively better mPFS in HER + HR− cohort compared to HER + HR + cohort and OS, although not significant (Fig. S1E). Accordingly, in this study, four malignant molecular subtypes were identified based on the gene expression patterns of *ERBB2*, *ESR1*, *CALML5* and *TFAP2B*, after which their correlation with clinical outcomes was validated using data from the Cancer Genome Atlas (TCGA) (http://gepia2.cancer-pku.cn/#survival). We then further determined the unique gene expression pattern in tumor cells attributed to therapeutic response to KN026. The scores within tumor cells with OR showed high expression of *ERBB2*, *CALML5* and *TFAP2B*, combined with low expression of *ESR1* compared with those of non-OR (p <0.01, Fig. 2a). We found that the negative association between the mRNA level of *ERBB2* and *ESR1*, as well as the positive association between *CALML5* and *TFAP2B*, especially in tumor segmentation regions with OR (r^2 = 0.26, $p < 0.01$; r^2 = 0.9, $p < 0.01$, Fig. 2b). We have explored the potential mechanisms of CALML5 and TFAP2B using the TCGA-BRCA dataset. The dataset analysis revealed that these two genes exhibit a significant positive correlation in normal breast tissues, whereas no obvious correlation was observed in cancer tissues (Fig. 2c). In the GDSC database, we also found that the drug sensitivity patterns of CALML5 are consistent with those of ERBB2, implying that CALML5 may be associated with the ERBB2 signaling pathway, although research on TFAP2B was limited (Fig. 2d).

Given the abundance of *ERBB2* expression across discrete tumor regions with OR as well as non-OR, we also found a consistent pattern of *ERBB2*-expressing cell populations in the tumor core, tumor margins and tumor microenvironment (Fig. S1F and G). We conjectured that the difference of therapeutic response cannot be entirely explained by intratumoral diversity of *ERBB2* expression. Therefore, we searched for the unique cancer-cell state characterized by the activation of ERBB2, TNF and NF-κB signaling pathways based on scored gene sets, which corroborated the existence of the higher proliferation state signatures involving estrogen, mTOR, Wnt, and P53 signaling pathways within tumor cells with non-ORR compared to OR (p <0.01, Fig. 2e-g). When we scored dynamical manifestation of tumor cells from tumor microenvironment interactions, the UMAP analysis revealed disseminated biological profiles of conserved *ERBB2* expression stratified by scoring of 1–3 (Fig. 2h). We found that multiple localization with *ERBB2* expression showed substantial correspondence to immuneScore

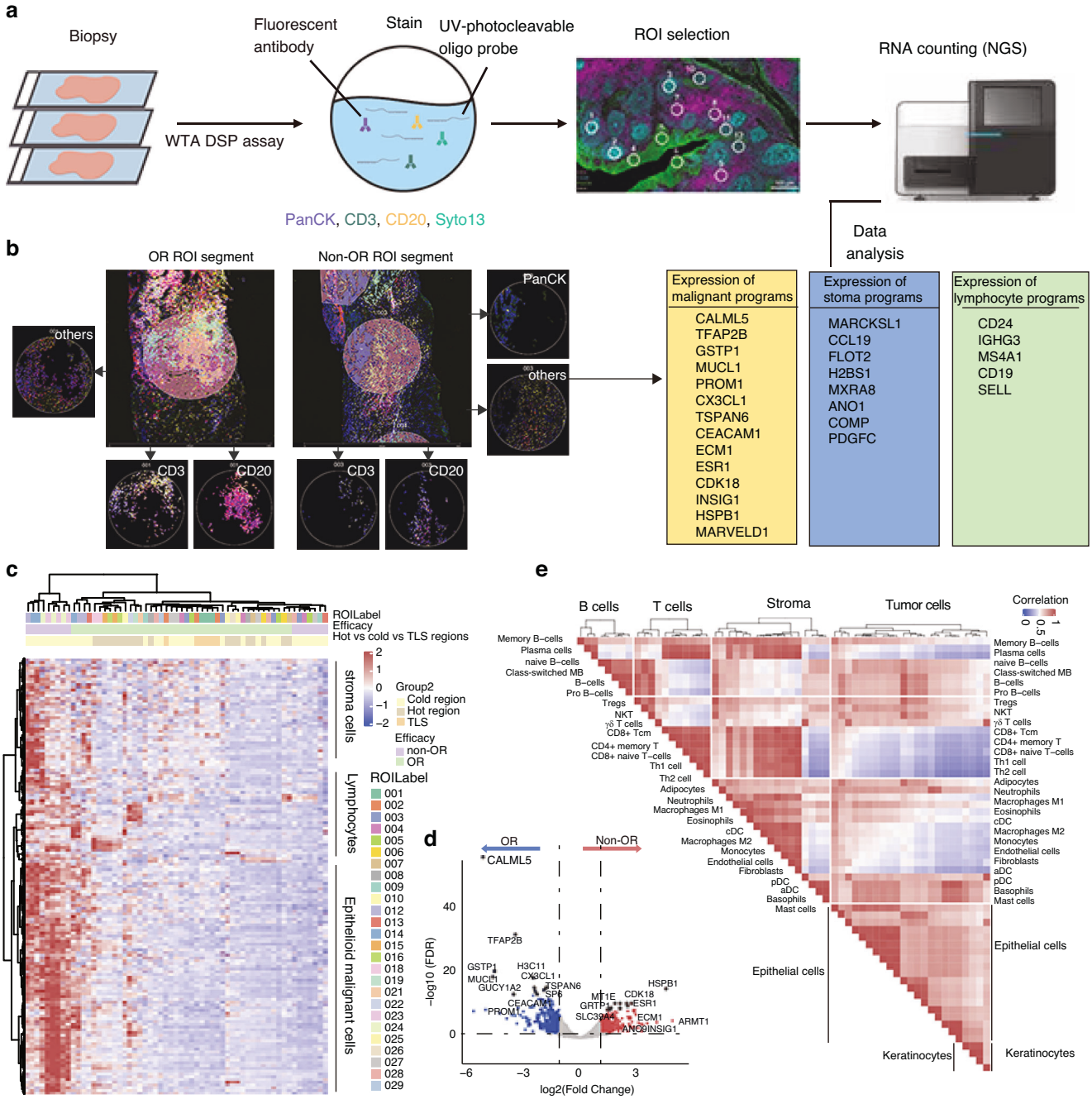

Fig. 1 Digital spatial profiling of archived formalin-fixed paraffin-embedded KN026-treated breast cancer primary lesions. a Schematic workflow of patients with HER2-positive breast cancer enrolled in the phase II multicenter clinical trial analyzed with the DSP (NanoString GeoMx). **b** Segmentation of multiple ROIs based on panCK, CD20, and CD3 staining and subjected to next-generation sequencing. Genes in function programs were listed. **c** DSP captures distinct malignant and lymphoid programs regarding the regions and efficacy. Mean normalized expression (color bar) of selected marker genes (columns) across multiple annotated compartments (rows). **d** Volcano plot demonstrated treatment-associated changes in tumor cells based on a comparison of RNA expression levels in Pan-CK-enriched regions in tumor with objective response and non-objective response. **e** Pearson correlation coefficient (color bar) of the scores/proportions of each malignant, B cell, T cell, and stroma subtypes (rows, columns) across ROIs. Rows and columns are ordered by hierarchical clustering.

(r^2 = 0.06, $p = 0.028$) and microenvironmentScore (r^2 = 0.08, $p = 0.015$) (Fig. 2i). In addition, high HER2-expressing tumor cells (3 +) displayed higher gene-set involved in estrogen signaling and drug metabolism (Padjå 0.05). Conversely, low HER2-expressing tumor cells (2 +) were characterized by gene sets involving in Th17 differentiation, Th1/Th2 differentiation and transendothelial leukocyte migration signaling (Padj < 0.01, Fig. 2j). Thus, cellular function hallmarks implied therapeutically responsive properties.

CDK12 and *ESR1* transcriptional level indicated spatially defined tumor cell populations with distinct therapeutic responses

We explored the gene set most related to *ERBB2* and found that expression of the cell cycle gene *CDK12* displayed consistent correlations with *ERBB2* within tumor cells in all tumor ROIs with OR ($r^2 = 0.057473$, $P = 0.037$, Fig. 3a, b). Correspondingly, KN026 treatment considerably decreased the expression of *CDK12* and

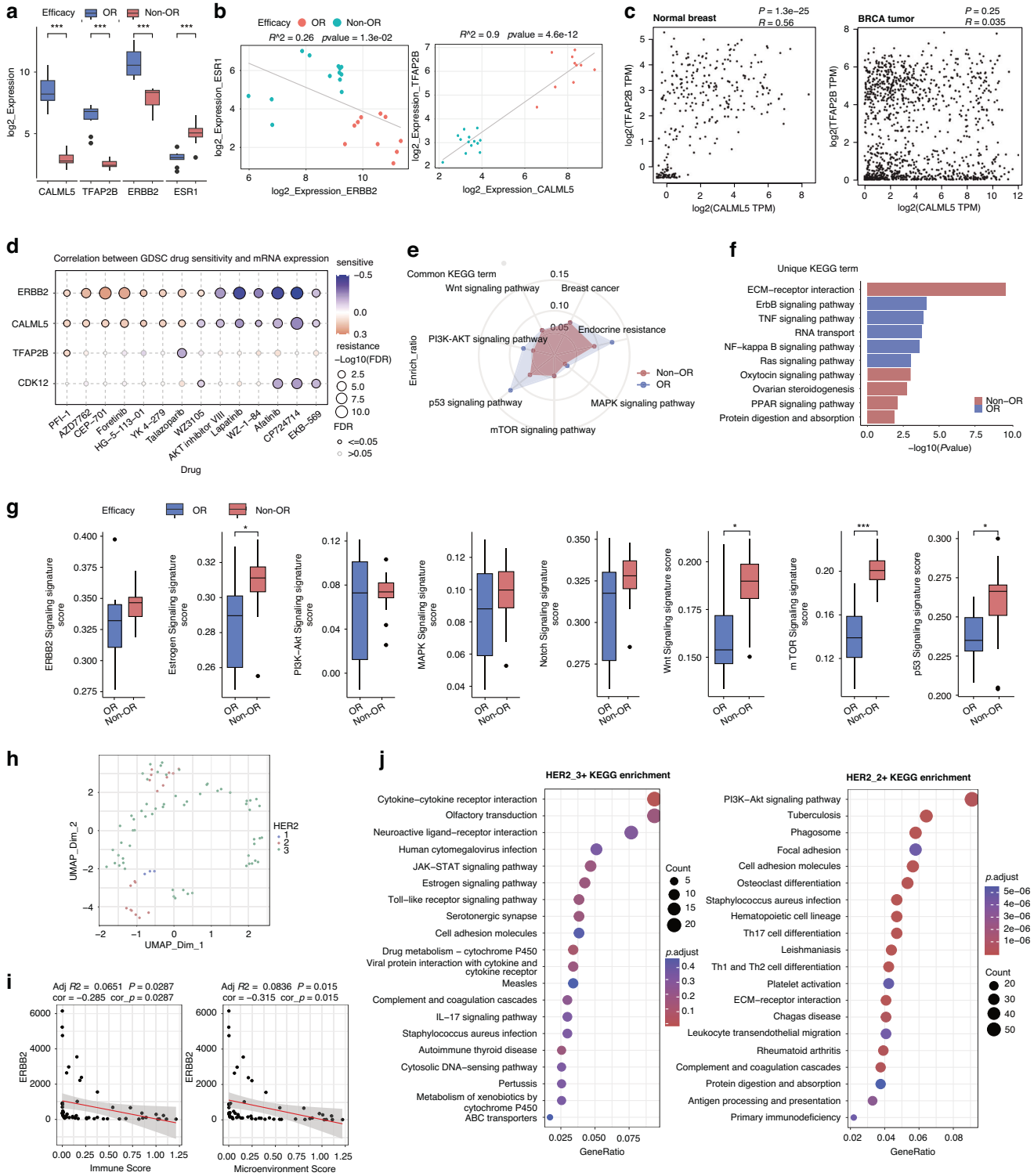

Fig. 2 Identification of baseline malignant signatures in distinct responsive regions to KN026 treatment. a Boxplots of DSP gene expression in prior treated transcriptional level stratified by response utilizing top significance of *CALML5, TFAP2B, ERBB2*, and *ESR1*. **b** Scatterplots comparing the normalized *ERBB2* expression to *ESR1* expression and normalized *TFAP2B* expression to *CALML5* expression. Two-sided test for association using Pearson's correlation coefficient, r; p value shown on plots. **c** Pearson Correlation analysis between CALML5 and TFAP2B using the TCGA-BRCA dataset. **d** Pearson correlation analysis between drug sensitivity and mRNA expression using GDSC dataset. **e** Radar plots and **f** bar chart showing common and unique Kyoto Encyclopedia of Genes and Genomes (KEGG) enrichment across tumor regions stratified by response, respectively. **g** Boxplots estimated critical growth signaling signatures stratified by response. **h** Uniform manifold approximation and projection (UMAP) embedding of single *ERBB2* profiles (dots) of treated tumors colored by HER2 IHC statues (color legend, right). **i** Scatterplots comparing the normalized *ERBB2* DSP RNA expression to the immune and microenvironment scores. The grey shading indicates the 95% confidence interval of the correlation coefficient. **j** Bubble plots comparing obvious inflammatory or metabolism pathways based on KEGG enrichment stratified by HER2 status. Two-sided test for association using Pearson's correlation coefficient, r; *p* value shown on plots.

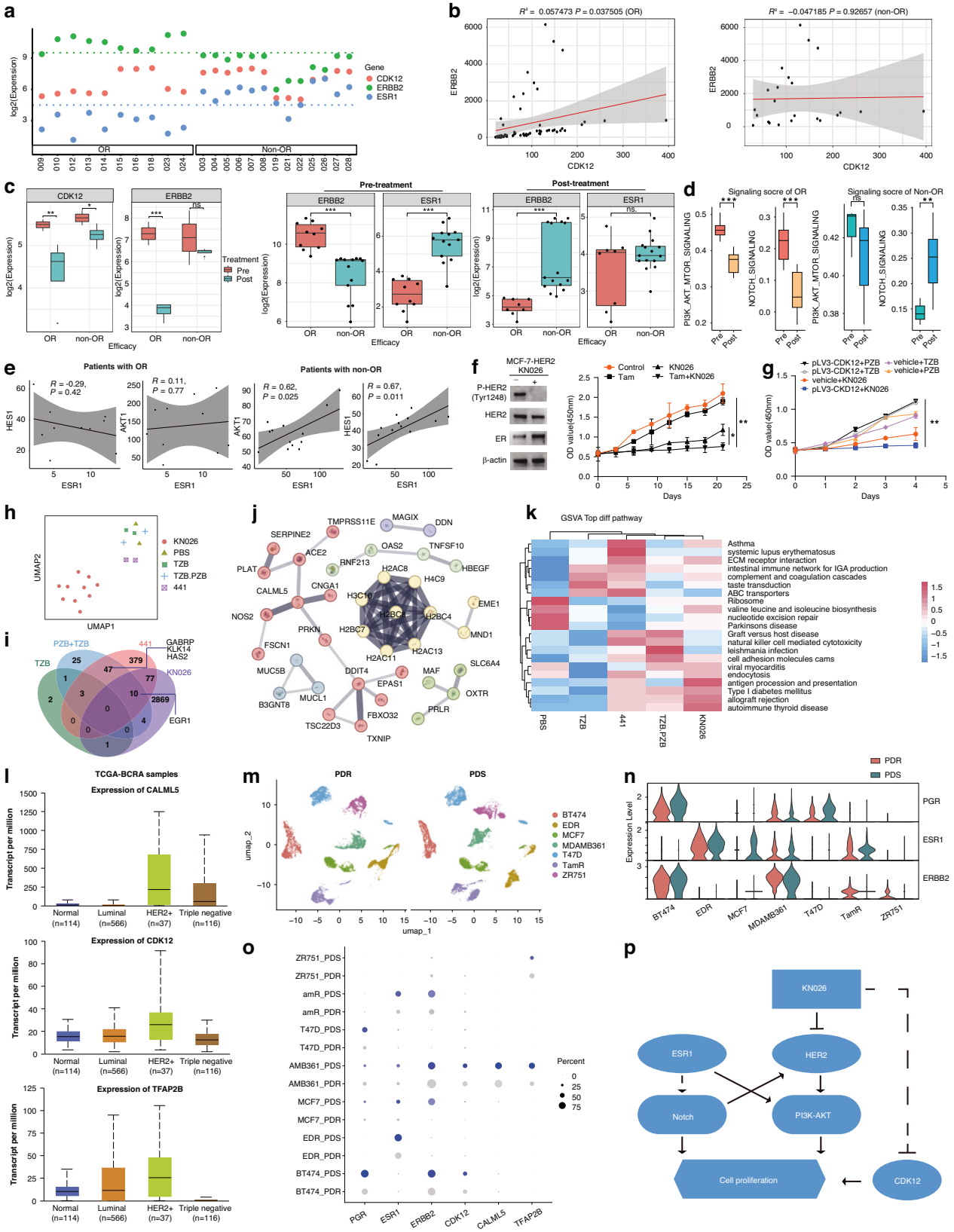

ERBB2, especially in tumor cells with OR. Interestingly, the previously-obvious difference in *ESR1* mRNA level between tumor cells with and without OR was significantly reduced after treatment, providing corroborative evidence of the effect on ER signaling from KN026 (Fig. 3c). We then investigated the contribution of the *ESR1* expression pattern for therapeutic responses. We found that outgoing signaling patterns decreased dramatically in tumor cells with OR after KN026 treatment,

Fig. 3 The classification of critical targets in tumor cells and exploration of potential mechanism of KN026 efficacy. a Scatterplot illustrated prior gene expression profile including *ERBB2, CDK12* and *ESR1* stratified by response, where each point corresponds to an ROI. **b** Scatterplots comparing the normalized *ERBB2* expression to *CDK12* expression within PanCK+ tumor cells in tumor with OR and non-OR respectively. Two-sided test for association using Pearson's correlation coefficient, r; *p* value shown on plots. **c** Data graphed as boxplots indicating differences in pre-treatment and post-treatment expression changes of *ERBB2, CDK12* and *ESR1* genes, as well as comparison between tumor with OR and non-OR. **d** Boxplot compared the changes of PI3K/AKT/mTOR and NOTCH signaling signatures within tumor cells following treatment in tumor with OR and non-OR. **e** Scatterplot comparison of mean DSP log2 negative-normalized expressions between ESR1 signaling and PI3K or NOTCH signaling within region of interest (ROI) in tumor with OR and non-OR. Two-sided test for association using Pearson's correlation coefficient, r; p value shown on plots. **f** A panel of HER2-overexpressing ER-positive breast cancer cell line was treated with KN026 (100 μg/ml) for 48 h and whole-cell extracts were analyzed by western blotting with indicated antibodies. CCK8 assay evaluated the inhibition rate blocked by single or combined treatment of tamoxifen (1 μM) and KN026 (100 μg/ml). *P* values are based on One-way ANOVA test. **g** CCK8 assay evaluated the inhibition rate blocked by single or bispecific antibodies derived from constructed CDK12-amplified HER-2-overexpressed tumor cell lines. *P* values are based on One-way ANOVA test. **h** UMAP clustering showed the principle components between anti-HER2 antibodies. **i** Venn diagram illustrated that The KN026-treated tumor included 'growth enhanced' genes such as *EGR1* programs from the tumor treated with trastuzumab and pertuzumab combinations, and 441. Overlap between the KN026 (purple), trastuzumab and pertuzumab (blue) and 441 (pink) genes ($n = 10$, $P = 1.29 \times 10 - 4$; two-sided hypergeometric). **j** PPI network illustrated the 77 differential expression genes shared between KN026 and 441. **k** Heatmap extracted the most significant KEGG pathways for each group. **l** Diagram showed the expression levels of CDK12, CALML5, and TFAP2B across different breast cancer subtypes using TCGA-BRCA data. **m** UMAP analysis characterized the expression levels of CDK12, CALML5, and TFAP2B in various breast cancer cell lines using the GSE298567 single-cell dataset and quantitated using violin plot (**n**) and Bubble diagram (**o**). **p** Illustrations depicted the mechanism of action of KN026 within breast cancer tumor cells. *p* value *$p < 0.05$, **$p < 0.01$, ***$p < 10$^3, ****$p < 10$^4.

including PI3K-AKT signaling (P_{adj}=8.8E-03) and NOTCH signaling (P_{adj}=1.60E-06). Simultaneously, NOTCH signaling (P_{adj}=0.0049) increased substantially in tumor cells with non-OR (Fig. 3d). A high degree of positive correlation was generally observed between estrogen signaling (*ESR1*) and NOTCH signaling (*HES1*, $r = 0.62$, $P = 0.025$, Pearson correlation coefficient) or PI3K-AKT signaling (*AKT1*, $r = 0.67$, $P = 0.011$) in tumor cells with non-OR, but the missing correlation between them within each tumor cell with OR, highlighting the potential bypass interaction between these signalings (Fig. 3e).

Next, we treated an HER2 and ER double-positive breast cancer cell line (MCF-7-HER2) with KN026 (100 mg/L), which resulted in a significant reduction of phosphorylated HER2 (Tyr1248) and upregulation of ER after 48 hours of treatment. We considered that the induction of ER activity could potentially explain the relatively better mPFS in HR-negative cohort of our subgroup analysis [5]. We therefore investigated the effect of a combined regimen with KN026 and ER-antagonist tamoxifen (1 mg/L). Interestingly, we observed significantly higher proliferation inhibition using this combined regimen compared to single drug treatment (Fig. 3f).

Previous work revealed *HER2* and *CDK12* co-amplification in TCGA data from the cBioPortal database (http://www.cbioportal.org) and METABRIC dataset [16], as well as the results from phase I clinical trial of KN026 [4], which was consistent with our correlation analysis of mRNA expression between them (Fig. S2A). We further characterized tumor cells with OR with decreased frequency of DNA repair after KN026 treatment, which is associated with CDK12 (Fig. S2B). We also found that KN026 treatment presented better proliferation inhibition in the HER2-positive breast cancer cell (BT474) with transfected CDK12 upregulation, compared with other HER2-targeting regimens such as trastuzumab or pertuzumab ($P = 0.038$, $P = 0.025$, respectively, Mann–Whitney, Figs. 3g; S2C). Our analysis indicates that *CDK12* and *ESR1* contributed to predicting the tumor cell response to KN026.

Unique tumor expression profiles following KN026 treatment

We sought to elucidate the special features of KN026, compared with other HER2-targeting drugs, such as the engineering anti-HER2 biparatopic antibody 441 (www.genewiz.com), TZB and PZB [17]. Dimensionality analysis showed the unique differentially expressed gene (DEG) clustering of KN026 distinguished from others (Fig. 3h, S2D). The *ERG1* expression in tumor cells exhibited high cellular contribution across all dual anti-HER2 antibody agents (Fig. 3i and Table S6). Furthermore, we conducted PPI network analysis on the 77 differential expression genes shared between KN026 and 441. The results revealed that both bispecific antibodies affect genes involved in chromatin remodeling and oxidative stress (Fig. 3j). Severally, translational initiation, targeting to ER, and neutrophil extracellular trap formation were most obviously seen in KN026-treated tumors (Fig. S2E). Only Notch signaling along with antigen processing and presentation was obviously upregulated in TZB-treated tumors (Fig. S2F). Natural killer (NK) cell-mediated immunity and cytotoxicity were prominent in combined TZB and PZB treatment (Fig. S2G). Several factors related to matrix stiffness, including collagen, and fibroblast growth factor receptor were consistently observed following both KN026 and 441 treatments (Fig. S2E, H). Heatmap visualized the most significant pathways and reinforced the clustering similarity between KN026 and other bispecific antibodies (441, TZB and PZB) (Fig. 3k).

To mitigate sample size limitations, we first analyzed the expression levels of CDK12, CALML5, and TFAP2B across different breast cancer subtypes using TCGA-BRCA data. The results showed that all three genes are highly expressed in HER2-positive breast cancer, which may imply an association between CDK12/CALML5 and the HER2 pathway (Fig. 3l). Furthermore, we characterized the expression levels of CDK12, CALML5, and TFAP2B in various breast cancer cell lines using the GSE298567 single-cell dataset (Fig. 3m). We found that BT474 and MDA-MB-361 cell lines, which have high ERBB2 expression, also exhibit high expression levels of CDK12, CALML5, and TFAP2B. Moreover, their expression levels are higher in the PDS group (wild-type) than in the PDR group (drug-resistant) (Fig. 3n, o). These findings are consistent with the results of our study, suggesting that high expression of CALML5 and TFAP2B may be associated with a higher likelihood of drug benefit and longer prognosis in patients.

We next delineated a backbone mechanism among malignant cells responding to KN026 treatment (Fig. 3p). The crosstalk between the core HER2 epitope and *ESR1*, the corresponding activated downstream PI3K-AKT and NOTCH signaling, as well as bypass *CDK12* signaling was attributed to specific reprograming of HER2-related pathways. Thus, strong inhibition of downstream of HER2 signaling from KN026 therapy could indirectly weaken the compensation effect of same pathways from ESR1-related signaling crosstalk (disadvantages) [18], explaining the similar benefit among HR subgroup.

Activated immune cells from KN026 treatment inhabit the responsive tumor regions

We next shifted our focus to immune cell repertoire, recognizing their crucial roles in tumor control during treatment responses (Fig. 4a, b). For example, ROI 002 and 012 in patient2 with OR may be the source of response, containing $CD8^+$ Tcm, cytotoxic T-cell,

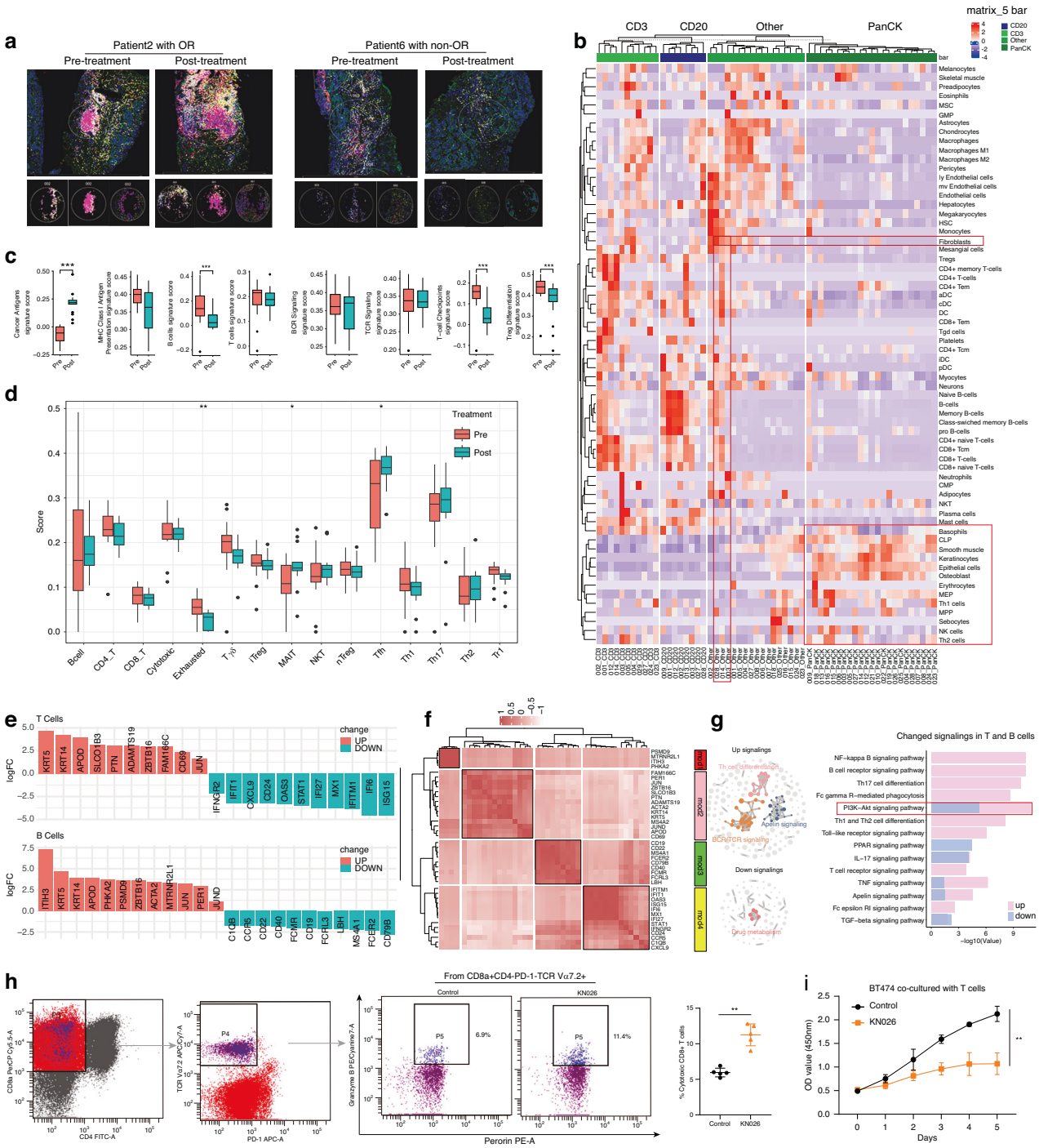

Fig. 4 Intratumoral immune infiltrations within full-tumor sections following KN026 treatment. a Representative images of segmented ROIs from two cases (OR vs non-OR) based on morphological staining of PanCK, CD3, and CD20 markers for intuitive comparison of treatment-related changes. **b** Heatmap of 29 individual ROIs comparing immune cells clustered in regions based on morphological segments on the x axis; red box depicts the most immune cell subtypes interacted with tumor cells. **c** Boxplots compared critical activation signalings within T cells and B cells in the cases of matched treated samples. *P* values were derived using a two-sided Wilcoxon rank-sum test. **d** Signature scores (y-axis) of cell types and cell states (x-axis) in responder tissues out of all T and B cell subsets in pre-treated versus post-treated tumor regions from OR. **e** Waterfall plots illustrating functional genes expression changes in T cells and B cells within tumor with OR following treatment. **f** Pairwise correlation of DEGs in T and B cells from tumor with OR following treatment. The black squares represent hierarchical clusters for modular division. **g** Pathway enrichment among DEGs of T cells and B cells following treatment. Left: comparison between critical up- and down-pathways within TME following effective treatment. Right: comparison of significant changed signalings in T and B cells. **h** Flow cytometry plots showing perforin+ and granzyme+ CD8 + T cell subset gated on all cytotoxic T cells (CD8a+TCR Vα7.2 + CD4-PD-1-). Proportion of perforin+ granzyme+ cytotoxic T cells subsets from treatment and control groups. Data points represent values from 5 individual co-cultured well and lines represent means ± SD. Statistical analysis using the Mann–Whitney test. **i** Cell viability of BT474 assessed by CCK8 assay in response to KN026 (100 μg/ml) treatment co-cultured with cytotoxic T cells. Triplicate measurements per group, and p values correspond to the Student's t-test.

and naïve T-cell signatures within a B-cell clustering neighborhood (CD20-postive segmentation). From ROI 028 and 014 in patient6 (non-OR) to ROI 003 in patient2, decreased fibroblasts were observed, reflecting different stroma hardness related to effective immune cell infiltration. Interestingly, PanCK-enriched tumor cells were in close proximity to Th1 and NK cells in ROI 015 and 018 of patient3 with OR.

To identify the immune cell-fate plasticity in effective treatment, we quantified the lineage classifications of immune cells among tumor regions with OR. We found substantially decreased abundance of regulatory T cells (Tregs) (P_{adj}=0.0016; Mann-Whitney-Wilcoxon test) and increased $CD4^+$ resting memory T cells (P_{adj}=0.0027). The decrease abundance of M1 macrophages (P_{adj}=0.0047) and NK cell clusters (P_{adj}=0.0388) implied that the tumor was devoid of the antibody dependent cell-mediated cytotoxicity (ADCC, Fig. S3A). An immune hallmark and key activation pathway-associated signature within these compartments was characterized by decreased T-cell checkpoint activity, Treg differentiation and B-cell signaling (Fig. 4c). Given the significance of lymphoid lineage with concurrent active signaling, we next focused on T and B cell lineages, revealing specific decreased exhausted scores, as well as increased MAIT and Tfh following effective treatment (Fig. 4d). Top DEGs within changed T cells included genes in four enriched modules involved in inflammation, including *JUN*, *CD69* in module 2 as well as *IFI6, STAT1*, and *IFNGR2* in module 4 (Figs. 4e, f; S3B; Table S7). Cellular function hallmarks that were upregulated in T cells included differentiation and response to type I interferon (Fig. S3C). By contrast, top genes in changed B cells included differentiation-related *JUND*, *PER1*, and *ZBTB16* in module 2, as well as inflammation-related *C1QB* and *CCR5* in module 4 (Figs. 4e, f; S3D; Table S8). Antigen presentation and regulation of myeloid cell differentiation signaling were upregulated in B cells (Fig. S3E). It is worth noting that growth- and glucose metabolism-related PI3K-AKT signaling was obviously increased in both T and B cells (Fig. 4g). After co-cultured T cells with BT474, KN026 treatment increased the proportion of CD8a + CD4-PD-1-TCR-Vα7.2+Perforin + Granzyme B+ cytotoxic T cells and inhibited the proliferation of tumor cells, indicating the reprogramming T cells with enhanced tumor-killing ability (Fig. 4h, i).

Considering HER2 heterogeneity, we compared the HER2 3+ regions with low HER2 expression regions (1 or 2 +) and showed the relative less co-expression with the majority of infiltrating immune cells especially pDC, iDC, MSC, mast cells and Tregs (Figs. 5a, S4), especially Tfh (Fig. 5b), implying the obvious immune exclusion the HER2-overexpressed regions. As for efficacy comparison, the obvious distinct immune cells among disparate regions of OR and non-OR areas were fibroblasts and NK cells (Fig. 5a). After strictly classifying two clusters of NK cells (activated and resting), there were inconsistent changes of proportions following treatment. Overall, activated NK cells were most highly enriched in stromal regions of non-OR, while the stromal regions of OR were enriched for resting NK cells (Fig. 5c). We found no significant differences in the expression of canonical NK cytotoxicity markers (*GNLY, GZMA, GZMB, GZMK*, and *NKG7*) in all ROIs (Fig. 5d). NK cells within disparate ROIs were scored for the correspondence to *ERBB2* expression signatures. We found that multiple NK cells may be present across all *ERBB2*-expressing regions (Fig. 5e). We next examined fibroblasts and found their prominent clustering at the tumor margin of non-OR areas, with higher numbers of neighboring spots enriched for tumor cells than in OR areas (Fig. 5f). Multiple fibroblasts may be co-localized in relatively low *ERBB2*-expressing regions (Fig. 5g), highlighting the regional architecture that impedes cell infiltration and drug diffusion into the tumor core.

Thus, distinct patterns of the tumor microenvironment enable further explanation of the unique efficacy of KN026 treatment in HER2-positive recurrent or metastatic breast cancer breast cancer.

DISCUSSION

Here, based on promising efficacy of KN026 treatment in HER2-positive recurrent or metastatic breast cancer, we investigated some source of preponderance distinguished from results of the PERUSE and PUFFIN studies [6, 7]. Prominently, our subgroup analysis results stratified by HR IHC finding showed similarity in survival benefits, but it demonstrated prolonged median PFS in both two cohorts beyond that of PUFFIN study among Chinese population [5, 12]. This manifestation raised our intriguing topic to expand a more diverse molecular profiling, facilitating to understanding and broadening of KN026 applicability.

The combination strategy with single HER2-targeting regimens involving in TZB and PZB was trying to break through the double inhibition effect in HER2 signalings [11], and KN026 as a bispecific antibody drug might achieve this goal [5]. Previous phase I trials of KN026 study [4] for exploration of therapeutic markers demonstrated that concerted *HER2/CDK12* co-amplification identified in directly orchestrated well responsive tumor. However, 70% co-amplification occurred in the HER2-amplificated subtype based on PAM50 stratification (TCGA Network, 2012) and instead, individuals without co-amplification also have a PFS benefit [4]. We expanded examination of tumor cell dynamics, not restricted to HER2-directed activities [9]. Previously, this co-amplification effect was found to be associated with the cell cycle, mTOR, and DNA repair pathways [4], often viewed as pro-cancerous [19]. Particularly, *CDK12*, which is highly correlated with transcriptional elongation and DNA repair response signaling [16], where these signalings were considerably decreased in tumor cells following KN026 treatment. This indirect target bias revealed heterogeneous functional effects accompanying *ERBB2* and *CDK12* crosstalk, which may yield synergistic effects [20]. Importantly, our analysis primarily supports *ESR1* [21] as the core mediator in the interaction effect of the HER2 target [22]. This result provides a tentative approach for the maintenance of tumor growth signaling from *ESR1* activation [18], partially confirmed by the negative correlation result between *ESR1* and *ERBB2*, along with the positive correlations between ESR1 and NOTCH signaling [23] or PI3K-AKT signaling [24]. Simultaneously, these two pathways are the downstream signaling of HER2 targets. Due to the strong inhibition of these two signalings from KN026, we could see the attenuated disadvantages from ESR1 compensation and partially explain the little survival distinction among HR subgroups.

Echoing the developing bispecific antibody strategy [17, 25], our study helps elucidate the priority of clinical application underlying successful KN026 treatment. Compared with extensive metabolism and adhesion signaling in the responses to TZB + PZB or dual antibody 441 [17], the release of HER2 internalization is relatively prominent in the KN026 regimen. Analogously, our quantified efficacy-related expression signature included *CALML5*, which was regarded as a risk factor in the treatment of HER2 + HR + breast cancer [26] and may influence carcinogenesis by ubiquitination. Moreover, *CALML5* was found to have a strong positive correlation with *TFAP2B* which mediates tumor proliferation, apoptosis and invasion [27]. The synergistic expression of *CALML5/TFAP2B* molecules increase the likelihood of beneficial outcomes of KN026 and could be predictive factors.

Interestingly, we found that within the tumor core, there are lower proportions of myeloid lineages which seems like a paradox of traditional opinion involving in antibody-dependent cellular cytotoxicity in antibody-type drugs relying on innate immunity [28]. Simultaneously, the dysfunction of NK cells with decreased expression of cytotoxicity-related gene sets suggests the impairment of natural-killing capacity, which reminiscent of broader immunoregulatory network to compensate this immune anergy. Thus, we discovered the preexisting immunocyte chemotaxis and migration signaling network which fostered a robust T- and B-cell migration into tumor areas. We speculate that immune reprogramming [29, 30] occurs in substantial lymphoid lineages with

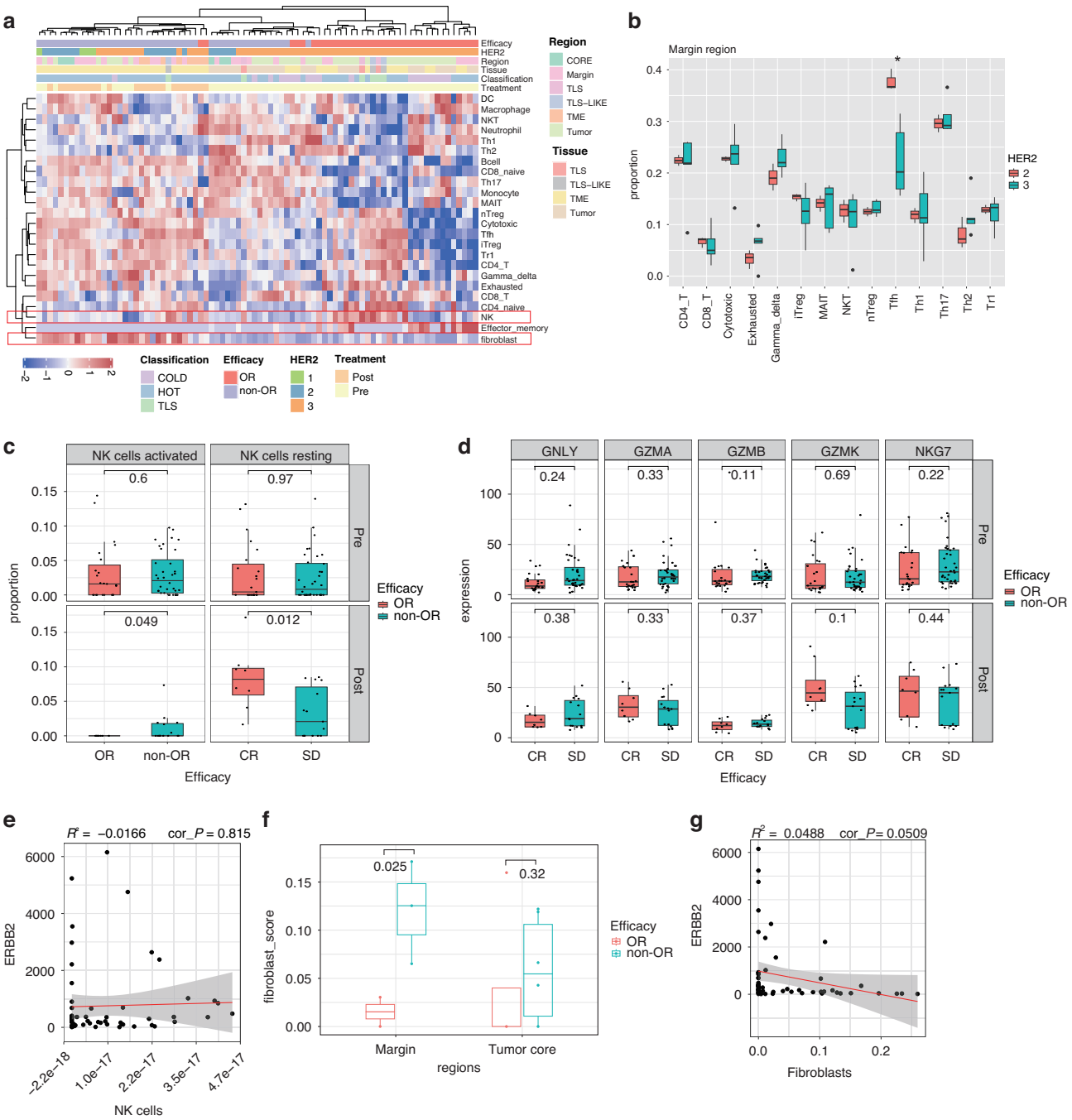

Fig. 5 DSP describes immune cells with striking difference in distinct TME regions related to treatment response. a Heatmap of DSP immune cells classifications across TME regions and comparison between tumor with classification of HER2 expression, efficacy, TME regions and treatment. Red frame line represented the immune cells with the most striking differences. **b** Boxplots compared T cell subtypes in the tumor margin area across different HER2 expression groups. P values were derived using a two-sided Wilcoxon rank-sum test. **c** The comparison of proportions in two NK cell subtypes following treatment. **d** The changes of five cytotoxic genes of NK cells following treatment. **e** Scatterplot comparison of single gene ERBB2 mean DSP log2 negative-normalized expression with NK cells signatures. Two-sided test for association using Pearson's correlation coefficient, r; *p* value shown on plots. **f** Boxplots compared the DSP mean fibroblast_scores between tumor margin and tumor cores in tumor with OR vs non-OR. **g** Scatterplot comparison of single gene ERBB2 mean DSP log2 negative-normalized expression with fibroblast signatures. Two-sided test for association using Pearson's correlation coefficient, r; *p* value shown on plots.

augmenting the T cell and B cell pool, which might result in functional activation in areas exhibiting treatment sensitivity. The high incidence of decreased exhausted lymphocytes associated with T-cell checkpoint signatures and Treg differentiation after treatment may unveil the alteration of antitumor immunity during TME-associated adaptation [31]. In addition, stromal cells such as cancer-associated fibroblasts produce a supportive extracellular matrix (ECM) with specific physical and chemical properties resulting in non-responsive features [32]. Our findings indicate that exclusion by fibroblasts at the tumor margin may be a crucial impediment for KN026 entering into the tumor core. Although we did not project subpopulations of CAFs, the global cell-oriented

profiles indicated more relevance for the trans-cellular molecular network mediating stroma hardness for infiltration of drugs or immune cells into the tumor. Our results fill gaps in existing research by explaining the spatial immune changes of lymphoid origin rather than innate immune system during KN026 treatment.

However, considering the small clinical sample size and lack of further verifiable data, these conclusions should be interpreted with caution until further validation in larger, independent datasets is available in subsequent large-scale experimental study.

Our analyses also invoke additional key question linked to promising combination treatment strategies with KN026, prominently combined with endocrine therapy for HER2 and ER double-positive breast cancer patients. We expect more clinical trials design in the future in a larger cohort for stronger evidence supports regarding this combination strategy.

CONCLUSIONS

In summary, we found that KN026 treatment reprogrammed the tumor and immune characteristics of patients toward a profile that facilitated the identification of limited beneficiary subgroups in advanced HER2-positive breast cancer. The selection of endocrine or other targeted drugs in conjunction with KN026 may have greater clinical significance, which warrants further exploration in the future.

TRANSLATIONAL REVELANCE

KN026 is a novel bispecific HER2-targeted antibody and confers a promising clinical benefit to HER2-positive breast cancer patients in our phase II clinical trial. The de novo mutation events only tended to explain the driver potentials. In order to elucidate subsequent changes in downstream pathways, using whole-transcriptome digital spatial profiling (DSP), we defined spatial multimolecular dynamic changes following KN026 treatment, including intensive crosstalks between HER2 and bypass signalings within tumor cells, and reversion of suppressive states in immune cells especially tumor infiltrating T and B lymphocytes, which interpreted the potential mechanism of the common efficacy regardless of HR status. Our work provides novel and detailed mechanistic insights into the superiority of KN026 efficacy, not only for the identification of advantageous populations, but also contributing towards combination strategy with endocrine therapy for advanced HER2- and HR-double positive breast cancer.

DATA AVAILABILITY

DSP datasets generated in the current study were published in Zenodo with https://zenodo.org/records/15354022. Data are now restricted ang will be also available on Zenodo as of the date of publication. Other data generated during the current study are available from the corresponding author.

REFERENCES

1. Bray F, Laversanne M, Sung H, Ferlay J, Siegel RL, Soerjomataram I, et al. Global cancer statistics 2022: GLOBOCAN estimates of incidence and mortality worldwide for 36 cancers in 185 countries. Cancer J Clin. 2024;74:229–63.
2. André F, Hee Park Y, Kim SB, Takano T, Im SA, Borges G, et al. Trastuzumab deruxtecan versus treatment of physician's choice in patients with HER2-positive metastatic breast cancer (DESTINY-Breast02): a randomised, open-label, multicentre, phase 3 trial. Lancet (London, England), 2023;401:1773-85.
3. Holmes FA, Moy B, Delaloge S, Chia SKL, Ejlertsen B, Mansi J, et al. Overall survival with neratinib after trastuzumab-based adjuvant therapy in HER2-positive breast cancer (ExteNET): A randomised, double-blind, placebo-controlled, phase 3 trial. European journal of cancer (Oxford, England: 1990), 2023;184:48-59.
4. Zhang J, Ji D, Cai L, Yao H, Yan M, Wang X, et al. First-in-human HER2-targeted Bispecific Antibody KN026 for the Treatment of Patients with HER2-positive Metastatic Breast Cancer: results from a Phase I Study. Clin Cancer Res: J Am Assoc Cancer Res. 2022;28:618–28.
5. Ma J, Wang J, Xu T, Ouyang Q, Wang X, Wang J, et al. Efficacy and safety of KN026 and docetaxel for HER2-positive breast cancer: a phase II clinical trial. Cancer Commun. 2025.
6. Miles D, Ciruelos E, Schneeweiss A, Puglisi F, Peretz-Yablonski T, Campone M, et al. Final results from the PERUSE study of first-line pertuzumab plus trastuzumab plus a taxane for HER2-positive locally recurrent or metastatic breast cancer, with a multivariable approach to guide prognostication. Ann Oncol J Eur Soc Med Oncol. 2021;32:1245–55.
7. Xu B, Li W, Zhang Q, Shao Z, Li Q, Wang X, et al. Pertuzumab, trastuzumab, and docetaxel for Chinese patients with previously untreated HER2-positive locally recurrent or metastatic breast cancer (PUFFIN): a phase III, randomized, double-blind, placebo-controlled study. Breast Cancer Res Treat. 2020;182:689–97.
8. Swain SM, Kim SB, Cortés J, Ro J, Semiglazov V, Campone M, et al. Pertuzumab, trastuzumab, and docetaxel for HER2-positive metastatic breast cancer (CLEOPATRA study): overall survival results from a randomised, double-blind, placebo-controlled, phase 3 study. Lancet Oncol. 2013;14:461–71.
9. Yang M, Li Y, Kong L, Huang S, He L, Liu P, et al. Inhibition of DPAGT1 suppresses HER2 shedding and trastuzumab resistance in human breast cancer. J Clin Investig. 2023;133:e164428.
10. Xu J, Ying J, Liu R, Wu J, Ye F, Xu N, et al. KN026 (anti-HER2 bispecific antibody) in patients with previously treated, advanced HER2-expressing gastric or gastro-esophageal junction cancer. Eur J Cancer. 2023;178:1–12.
11. Li Z, Metzger Filho O, Viale G, dell'Orto P, Russo L, Goyette MA, et al. HER2 heterogeneity and treatment response-associated profiles in HER2-positive breast cancer in the NCT02326974 clinical trial. J Clin Investig. 2024;134.
12. Xu B, Li W, Zhang Q, Li Q, Wang X, Li H, et al. Pertuzumab, trastuzumab, and docetaxel for Chinese patients with previously untreated HER2-positive locally recurrent or metastatic breast cancer (PUFFIN): final analysis of a phase III, randomized, double-blind, placebo-controlled study. Breast Cancer Res Treat. 2023;197:503–13.
13. Wang XQ, Danenberg E, Huang CS, Egle D, Callari M, Bermejo B, et al. Spatial predictors of immunotherapy response in triple-negative breast cancer. Nature. 2023;621:868–76.
14. Eisenhauer EA, Therasse P, Bogaerts J, Schwartz LH, Sargent D, Ford R, et al. New response evaluation criteria in solid tumours: revised RECIST guideline (version 1.1). Eur J Cancer. 2009;45:228–47.
15. Merritt CR, Ong GT, Church SE, Barker K, Danaher P, Geiss G, et al. Multiplex digital spatial profiling of proteins and RNA in fixed tissue. Nat Biotechnol. 2020;38:586–99.
16. Choi HJ, Jin S, Cho H, Won HY, An HW, Jeong GY, et al. CDK12 drives breast tumor initiation and trastuzumab resistance via WNT and IRS1-ErbB-PI3K signaling. EMBO Rep. 2019;20:e48058.
17. Kast F, Schwill M, Stüber JC, Pfundstein S, Nagy-Davidescu G, Rodríguez JMM, et al. Engineering an anti-HER2 biparatopic antibody with a multimodal mechanism of action. Nat Commun. 2021;12:3790.
18. Pegram M, Jackisch C, Johnston SRD. Estrogen/HER2 receptor crosstalk in breast cancer: combination therapies to improve outcomes for patients with hormone receptor-positive/HER2-positive breast cancer. NPJ Breast Cancer. 2023;9:45.
19. Filippone MG, Gaglio D, Bonfanti R, Tucci FA, Ceccacci E, Pennisi R, et al. CDK12 promotes tumorigenesis but induces vulnerability to therapies inhibiting folate one-carbon metabolism in breast cancer. Nat Commun. 2022;13:2642.
20. Yanai Y, Kosaka T, Nakamura K, Aimono E, Matsumoto K, Morita S, et al. CDK12 and HER2 coamplification in two urothelial carcinomas with rapid and aggressive clinical progression. Cancer Sci. 2020;111:4652–5.
21. Venetis K, Pepe F, Pescia C, Cursano G, Criscitiello C, Frascarelli C, et al. ESR1 mutations in HR+/HER2-metastatic breast cancer: enhancing the accuracy of ctDNA testing. Cancer Treat Rev. 2023;121:102642.
22. Vigano L, Locatelli A, Ulisse A, Galbardi B, Dugo M, Tosi D, et al. Modulation of the estrogen/erbB2 receptors cross-talk by CDK4/6 inhibition triggers sustained senescence in estrogen receptor- and ErbB2-positive breast cancer. Clin Cancer Res. 2022;28:2167–79.
23. Pandey P, Khan F, Choi M, Singh SK, Kang HN, Park MN, et al. Review deciphering potent therapeutic approaches targeting Notch signaling pathway in breast cancer. Biomed Pharmacother Biomed Pharmacotherapie. 2023;164:114938.
24. Dubey R, Sharma A, Gupta S, Gupta GD, Asati V. A comprehensive review of small molecules targeting PI3K pathway: exploring the structural development for the treatment of breast cancer. Bioorg Chem. 2024;143:107077.
25. Weisser NE, Sanches M, Escobar-Cabrera E, O'Toole J, Whalen E, Chan PWY, et al. An anti-HER2 biparatopic antibody that induces unique HER2 clustering and complement-dependent cytotoxicity. Nat Commun. 2023;14:1394.
26. Bu J, Zhang Y, Niu N, Bi K, Sun L, Qiao X, et al. Dalpiciclib partially abrogates ER signaling activation induced by pyrotinib in HER2(+)HR(+) breast cancer. eLife. 2023;12:e85246.
27. Fu X, Zhang H, Chen Z, Yang Z, Shi D, Liu T, et al. TFAP2B overexpression contributes to tumor growth and progression of thyroid cancer through the COX-2 signaling pathway. Cell Death Dis. 2019;10:397.

28. Li F, Liu S. Focusing on NK cells and ADCC: A promising immunotherapy approach in targeted therapy for HER2-positive breast cancer. Front Immunol. 2022;13:1083462.
29. Fernandez-Martinez A, Pascual T, Singh B, Nuciforo P, Rashid NU, Ballman KV, et al. Prognostic and predictive value of immune-related gene expression signatures vs tumor-infiltrating lymphocytes in early-stage ERBB2/HER2-positive breast cancer: a correlative analysis of the CALGB 40601 and PAMELA trials. JAMA Oncol. 2023;9:490–9.
30. Dolton G, Rius C, Wall A, Szomolay B, Bianchi V, Galloway SAE, et al. Targeting of multiple tumor-associated antigens by individual T cell receptors during successful cancer immunotherapy. Cell. 2023;186:3333–49.e27.
31. Cao T, Zhang W, Wang Q, Wang C, Ma W, Zhang C, et al. Cancer SLC6A6-mediated taurine uptake transactivates immune checkpoint genes and induces exhaustion in CD8(+) T cells. Cell. 2024;187:2288–304.e27.
32. Honda CK, Kurozumi S, Fujii T, Pourquier D, Khellaf L, Boissiere F, et al. Cancer-associated fibroblast spatial heterogeneity and EMILIN1 expression in the tumor microenvironment modulate TGF-β activity and CD8(+) T-cell infiltration in breast cancer. Theranostics. 2024;14:1873–85.

ACKNOWLEDGEMENTS

We thank all patients for providing specimens and medical history, and Kindstar Global Precision Medicine Institute (Shenzhen) for technical support. We are grateful to the Harbin Medical University Cancer Hospital for clinical data collection and sample provision. The authors would like to thank PaperArtist for providing English editing services during the preparation of this manuscript.

AUTHOR CONTRIBUTIONS

QZ and YD conceived and supervised the study. JM, SS and YD participated in bioinformatic analysis, trial monitoring, statistical analysis, data mapping, and drafting of the initial manuscript. XT performed data correction and collation. JW, WZ, DT, YS, and LL provided enrolled patients and clinical data, performed clinical management and collected clinical samples. HL and XL performed data supplementary from public datasets and bioinformatics analysis. JM, SS, YD and QZ reviewed and edited the manuscript. All authors have read and approved the final version of the manuscript.

FUNDING

This work was supported by a grant from Regional joint key project of National Natural Science Foundation (No. U22A20323), General Program of National Natural Science Foundation of China (No.82172780) and Outstanding Youth Project of the Natural Science Foundation of Heilongjiang Province (No. YQ2023H021).

COMPETING INTERESTS

The authors declare no competing interests.

ETHICS APPROVAL AND CONSENT TO PARTICIPATE

This study was approved by the institutional review board of Harbin Medical University Cancer Hospital (Approval no. 2019-180). All patients provided written informed consent forms. This study was performed in accordance with the Declaration of Helsinki.

ADDITIONAL INFORMATION

Supplementary information The online version contains supplementary material available at https://doi.org/10.1038/s41416-025-03287-9.

Correspondence and requests for materials should be addressed to Yuwei Deng or Qingyuan Zhang.